Optical beamsteering using an 8 × 8 MEMS phased array with closed-loop interferometric phase control

Trevor K. Chan,[1,*] Mischa Megens,[1] Byung-Wook Yoo,[2] John Wyras,[2] Connie J. Chang-Hasnain,[2] Ming C. Wu,[2] and David A. Horsley[1]

[1]*Department of Mechanical and Aerospace Engineering, University of California, Davis, One Shields Ave., Davis, California 95616, USA*

[2]*Department of Electrical and Computer Engineering, University of California, Berkeley, Cory Hall, Berkeley, California 94720, USA*

[*]*trechan@ucdavis.edu*

Abstract: We present a high-speed optical beamsteering system based on an 8x8 MEMS phased array. The system incorporates an in situ interferometer that provides a real-time, dynamic measure of the phase of each mirror in the array during beamsteering. A closed-loop phase-control algorithm results in $<\pi/100$ mirror phase accuracy and far field beam steering is shown. Stroboscopic measurement capabilities are demonstrated which allow us to show feedforward control to eliminate micromirror ringing.

OCIS codes: (060.2605) Free-space optical communication; (100.3175) Interferometric imaging; (110.5100) Phased-array imaging systems; (230.4685) Optical microelectromechanical devices; (230.6120) Spatial light modulators.

References and links

1. P. F. McManamon, P. J. Bos, M. J. Escuti, J. Heikenfeld, S. Serati, H. Xie, and E. A. Watson, "A review of phased array steering for narrow-band electrooptical systems," Proc. IEEE **97**(6), 1078–1096 (2009).
2. A. C. Clay, S.-C. Wooh, L. Azar, and J.-Y. Wang, "Experimental study of phased array beam steering characteristics," J. Nondestruct. Evaluat. **18**(2), 59–71 (1999).
3. D. P. Resler, D. S. Hobbs, R. C. Sharp, L. J. Friedman, and T. A. Dorschner, "High-efficiency liquid-crystal optical phased-array beam steering," Opt. Lett. **21**(9), 689–691 (1996).
4. B.-W. Yoo, M. Megens, T. K. Chan, T. Sun, W. Yang, C. Chang-Hasnain, D. A. Horsley, and M. C. Wu, "Optical phased array using high contrast gratings for two dimensional beamforming and beamsteering," submitted to Opt. Express.
5. V. Karagodsky, F. G. Sedgwick, and C. J. Chang-Hasnain, "Theoretical analysis of subwavelength high contrast grating reflectors," Opt. Express **18**(16), 16973–16988 (2010).
6. L. L. Chu and Y. B. Gianchandani, "A micromachined 2D positioner with electrothermal actuation and sub-nanometer capacitive sensing," J. Micromech. Microeng. **13**(2), 279–285 (2003).
7. J. Dong and P. M. Ferreira, "Simultaneous actuation and displacement sensing for electrostatic drives," J. Micromech. Microeng. **18**(3), 035011 (2008).
8. N. C. Singer and W. P. Seering, "Preshaping command inputs to reduce system vibration," J. Dyn. Syst. Meas. Control **112**(1), 76–82 (1990).
9. J. W. Goodman, *Introduction to Fourier Optics,* (McGraw-Hill Science/Engineering/Math, 1996), Chap. 4.
10. T. G. Bifano and J. B. Stewart, "High-speed wavefront control using MEMS micromirrors," Proc. SPIE **5895**, 58950Q, 58950Q–9 (2005).

1. Introduction

Optical phased arrays have been shown as viable options for beamsteering [1–3]. Phased array elements need only create phase delays within a wavelength due to the periodic nature of the light. This allows full field phase manipulation from a nearly flat device. In the case of beamsteering, a tilted mirror is equivalent to a blazed grating. The Huygens-Fresnel principle shows that this blazed grating can be approximated by a periodic staircase of segmented steps. Therefore, a phased array performs beamsteering by creating these periodic staircase patterns. Like a grating, a diffraction order exists according to the period of the staircase pattern.

#180849 - $15.00 USD Received 30 Nov 2012; revised 17 Jan 2013; accepted 22 Jan 2013; published 29 Jan 2013

The accuracy of beamsteering direction is a result of how accurate the phased array can reproduce the corresponding grating period. Both a finer phased array pitch and larger number or array elements result in more accurate beamsteering. The phase accuracy of individual array elements dictate the diffraction efficiency into the steered beam. For example, in the case of an 8x8 array, calculations reveal 3 dB diffraction efficiency loss in the steered beam results from $\pm 0.4\pi$ random phase error.

In our work, we have created an 8x8 array of high contrast grating (HCG) mirrors that use electrostatic actuation to create a variable phase delay. The design, fabrication and characteristics of these arrays are reported in [4]. The 8x8 version of this array was selected for this study since the individual voltage control of 64 mirrors is manageable while the total area of the array (280 x 280 μm) is large enough to limit the beam divergence to 5.5 mrad at c-band wavelengths. HCG mirrors hold the advantage of high reflectivity, wavelength insensitivity and light weight [5] which allows for unprecedented mirror actuation speeds. We design these mirrors to reflect 1550 nm light with 99% reflectivity and 20 V drive signal to produce at least 775 nm stroke (2π reflected phase shift). However, the ideal actuation response is rarely realized as reality introduces errors from fabrication and environmental influences during operation. These phase errors manifest themselves as a loss of diffraction efficiency and pointing accuracy. While these can and will be improved by refining the fabrication process, our goal here is to show that these problems are also corrected through our closed loop feedback operation.

This paper describes a high-speed optical beamsteering system based on the 8x8 MEMS phased array. The system incorporates an in situ interferometer that provides a real-time, dynamic measure of the phase of each mirror in the array during beamsteering. This holds advantages over capacitive sensing which is subject to parasitic capacitance from external instruments and requires large structures (e.g. comb drives) to achieve nanometer resolution [6, 7]. To compensate for slow, time-varying phase errors resulting from thermal and electromechanical drift in the optical system, a closed-loop phase-control algorithm ensures accuracy of the phase settings to achieve a desired far-field beam pattern.

2. Setup

The optical component of our system has three functions: 1) measure individual mirror reflected phase delays, 2) create a collimated beam on the phased array and 3) deliver a steered beam. Commercial microscopic interferometric imaging systems view the sample under a microscope objective which makes the latter two requirements difficult to realize, so we designed the optical assembly shown in Fig. 1.

We use a fiber collimating lens (Thorlabs PAF-X-5-C) and an additional focusing lens (AC254-150-C-ML, f = 15 cm) to create a collimated 332 μm diameter Gaussian beam that fits the MEMS device. This collimation requires two lenses (shown in the bottom arm of Fig. 1) to situate the device within the limited Rayleigh range.

The phase measurements are obtained through phase shifting interferometry (PSI). Our interferometer is composed of a series of a polarization beamsplitters and half wave plates to adjust the powers in the reference, measurement and output beams. Since we want to illuminate the device at normal incidence, we use a Faraday rotator to circulate the collinear reflected light through the adjacent polarization beamsplitter. The array is rotated 45° to match the incident polarization. A computer controlled Thorlabs Nanomax-600 stage supports and translates the MEMS device to produce adequate phase shifts for PSI. For microscopic imaging, we perform 4f image relaying with a pair of matched 10 cm focal length lenses to achieve 7.5 μm imaging resolution; sufficient to distinguish individual mirrors in the MEMS array. This image relaying system is necessary to keep the magnification microscope objective away from the sample and allow for steered output. The relayed image is magnified by a 10X microscope objective which forms the image on an InGaAs sensor array infrared (IR) camera (Xenics Bobcat-1.7-320) which is required to view 1550 nm wavelengths. The phase of each camera pixel is determined by translating the MEMS device using the stage and observing the resulting sinusoidal variation in intensity (PSI). We used 10 steps in triangular

#180849 - $15.00 USD Received 30 Nov 2012; revised 17 Jan 2013; accepted 22 Jan 2013; published 29 Jan 2013

fashion (5 forward and 5 back), covering one full period, and extracted the phase using a least squares fit. The frame rate of the camera and the speed of the translation stage enable a measurement of the displacement of all the MEMS mirrors about once every second. Since we are interested in only the mirror movements, any phase aberrations are removed by subtracting a reference phase map of the MEMS mirrors at rest. The camera is capable of stroboscopically measuring MHz MEMS movements with 80 ns frame integration times. Since we gate the image instead of the illumination source, the laser can be continuous and the system can maintain high power for beam steering.

The steered beam output of our device is separated at the top right corner in Fig. 1. At this point, the reflected device output is Fourier transformed by one of the image relaying lenses. To restore the steered beam, we use another confocal lens. By selecting a smaller focal length lens here, we can arbitrarily increase the total beamsteering field of view.

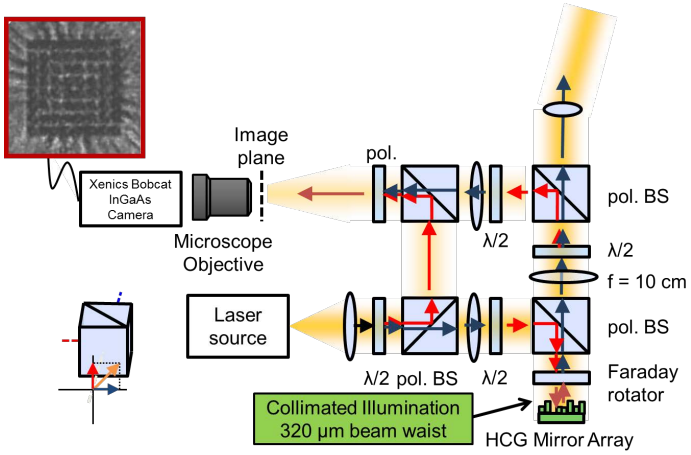

Fig. 1. Diagram of the optical system. A series of polarization beamsplitters and half wave plates form the two arms of an interferometer. Two lenses create a collimated illumination spot that fits the MEMS device. The measurement arm of the interferometer includes a 4*f* imaging system to preserve the imaging resolution and keep the imaging optics from blocking the steered device output. The output is extracted at the top right of the diagram, and magnified with a confocal lens with smaller focal length.

We can optionally remove the Faraday rotator to suppress background light reflecting from the wafer substrate. The mechanism behind this is as follows. Light reflecting from the background substrate maintains its polarization state which corresponds to the reflection mode of the polarization beamsplitter. The light from the HCG mirrors interacts with 45° rotated HCG mirror whose polarization dependence separates the light into two orthogonally polarized components. These are the HCG's TE and TM modes which now introduce power in the polarization beamsplitter's transmission path. There is an associated 3 dB loss from 45° polarized light passing through the polarization beamsplitter cube, but this tradeoff is acceptable when the device fill factor is small or when the array is overfilled by the illuminating beam spot.

Using our ability to measure the phase of each HCG mirror, we can adjust the control voltages to achieve the desired phase levels through closed loop control, as illustrated in Fig. 2. Here, the initial control voltage is generated from a look-up table. The closed loop control subsequently adjusts the voltage until the desired phase is observed. The speed of one iterative loop is limited by the long (~0.1 second) response time of the phase shifter required for PSI. Nevertheless, this speed is sufficient for initially setting and periodically updating the look-up table for initial device calibration and correction for long term drift.

#180849 - $15.00 USD Received 30 Nov 2012; revised 17 Jan 2013; accepted 22 Jan 2013; published 29 Jan 2013

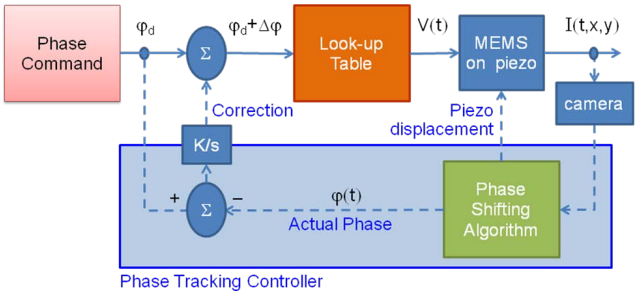

Fig. 2. Closed loop feedback control diagram. Control voltages are defined for phase setpoints with feedback control to compensate for long term drift.

3. System Characterization

3.1 Phase Measurements

Figure 3(a) shows a still frame of the interference pattern acquired by our imaging system with the Faraday rotator in place. Here, our HCG mirrors are 20 × 20 µm with 35 µm pitch to allow room for electrical lines to run between them. The mirrors are designed with 99% reflectivity, creating visible contrast with the surrounding Si substrate. The mirror edges appear blurred due to the 7.5 µm resolution limit; however, the individual mirrors are large enough to be distinguished. Through PSI, we calculate the phase change from the reflected light, shown in Fig. 3(b), as the mirrors are pulled down. Repeated measurements on a static device reveal π/250 measurement repeatability.

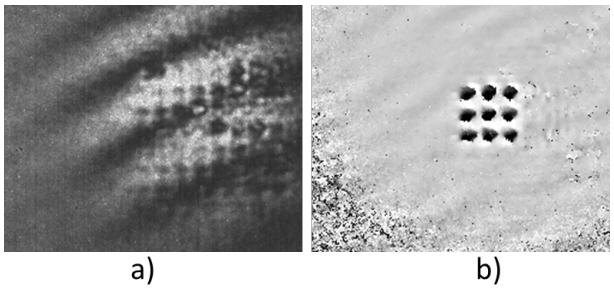

Fig. 3. (a) Raw interferogram image of the MEMS phased array and (b) the calculated phase map with the background subtracted and 18 V applied to nine adjacent pixels.

To track the mirror phase without introducing errors from the blurred mirror edges, we calculate the mean phase shift of the central area (approximately half the mirror area). Since all mirrors are visible on the camera, these calculations are done in parallel. Figure 4 shows the parabolic phase response with voltage of one mirror as measured by our system. Measurements of all the mirrors reveal two familiar problems in MEMS fabrication: a) mirrors do not have identical phase response and b) mirror crosstalk creates phase responses dependent on the setting of other mirrors. This means that open loop control, even with tedious calibration of every mirror, will fail to deliver accurate phase shifts and will subsequently produce a distorted far-field output with reduced diffraction efficiency. This highlights the importance of a closed-loop feedback method.

#180849 - $15.00 USD Received 30 Nov 2012; revised 17 Jan 2013; accepted 22 Jan 2013; published 29 Jan 2013

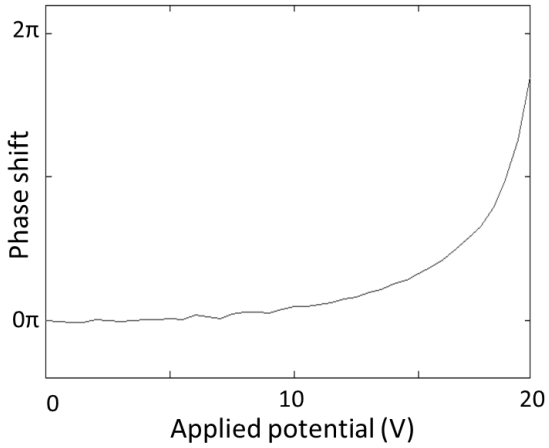

Fig. 4. Measured reflected phase shift from an actuated mirror.

3.2 Dynamic Oscillation Compensation

Our micromirrors are supported by elastic structures which exhibit damped harmonic oscillations that extend the mirror's settling time. Feedforward drive signal shaping can mitigate these oscillations and effectively minimize the slew rate for rapid beam steering [8]. Our Xenics Bobcat-1.7-320 imager can have short (<1 μs) integration windows to measure the mirror dynamic response stroboscopically. To measure the mirror dynamic response, we actuated a single mirror with a periodic square pulse that was synchronized to the 1 μs camera integration window. The square wave followed the camera trigger by a variable delay that was scanned to create a transient measurement. Our phase shift calculations from these images produce the transient response shown in the first plot in Fig. 5. This shows damped oscillation with a 1.82 μs damping time constant and 232 kHz resonance when the mirror is pulled down. The oscillation lasts only a few cycles, due to squeeze film damping of the mirror that is operating in air at atmospheric pressure. Even so, the sudden step results in a sizeable overshoot. To eliminate the oscillations, we applied a feedforward control signal consisting of two voltage steps. The elimination of ringing is accomplished by using an intermediate voltage step which makes the phase peak at our desired phase setpoint, then stepping the voltage again, right at the moment when the displacement is largest, setting the voltage to the final level which holds the mirror steady. The second half of Fig. 5 shows the corresponding transient response where the settling time is now reduced by more than an order of magnitude.

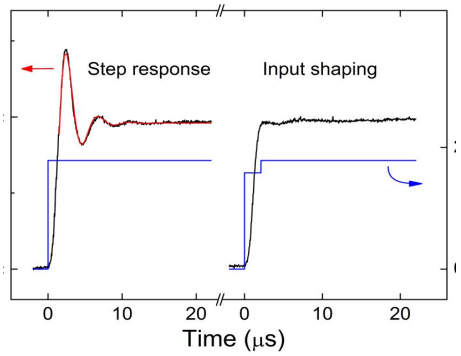

Fig. 5. Transient response of a mirror actuated with a voltage step and with a shaped signal to eliminate harmonic oscillations.

#180849 - $15.00 USD Received 30 Nov 2012; revised 17 Jan 2013; accepted 22 Jan 2013; published 29 Jan 2013

3.3 Feedback Control

Figure 6 reveals the feedback control ability of our system on a single mirror phase. In these measurements, we target a 1.0 π phase setpoint and adjust the device temperature using a thermoelectric cooler in contact with the device. Section I of the figure shows the voltage level being adjusted to maintain the phase level with approximately π/100 rms deviation. In section II, the voltage level is maintained to show how the mirror phase would drift under open-loop control. The drift is significant (0.2 π with 4°C temperature change) and further demonstrates the need for closed loop phase control. Section III shows closed-loop feedback used to restore the 1.0 π mirror phase. Note that the voltage level required to maintain 1.0 π phase at 21°C in section III has changed from section I despite the same device temperature. It is not yet clear why this occurs.

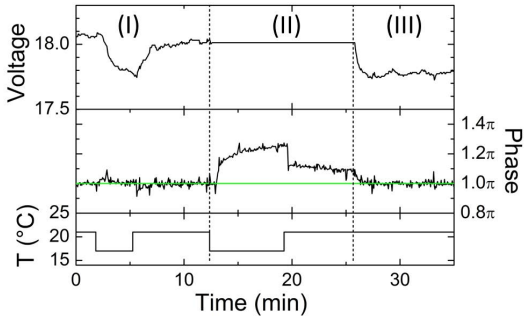

Fig. 6. Demonstration of phase control of a single mirror with a 1.0 π phase shift target. The plot shows three periods with closed-loop phase control on, off and on, respectively. The temperature is switched between 21°C and 17°C to induce a mirror response drift in the first two periods.

3.3 Beamsteering

We demonstrate the beamsteering ability of the phased array by imposing a diagonal phase gradient. This was set to steer the beam to half of the maximum achievable beamsteering angle defined by the Nyquist criterion. The desired and measured phase patterns are shown in Fig. 7. Due to mirror nonuniformity and crosstalk in these first generation devices, we are only able to achieve accurate phase patterns using the closed loop feedback system. Obviously, the dead mirrors remain stationary and appear with 0 phase shift in the measured phase pattern. Using the far field Fourier diffraction theorem [9], we show the expected far field pattern from a flat array in Fig. 8(a), the far field pattern when the phase gradient is applied in Fig. 8 (b), and the comparison of the two in a line plot in Fig. 8(c). Figures 8(d)–8(f) are the experimentally measured results corresponding to these calculations, captured by the camera. Since the observed angles are dictated by the magnification system, we normalized the angles according to the period of the phased array. We calculated the

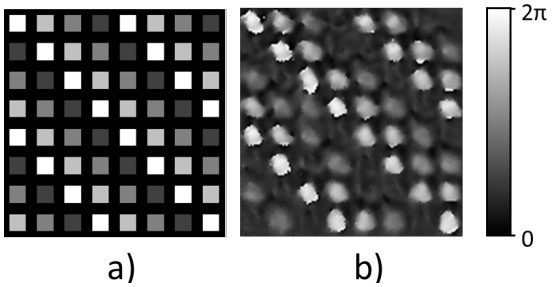

Fig. 7. (a) Target and (b) measured phase patterns. The measured phase pattern was achieved using closed loop feedback.

#180849 - $15.00 USD Received 30 Nov 2012; revised 17 Jan 2013; accepted 22 Jan 2013; published 29 Jan 2013

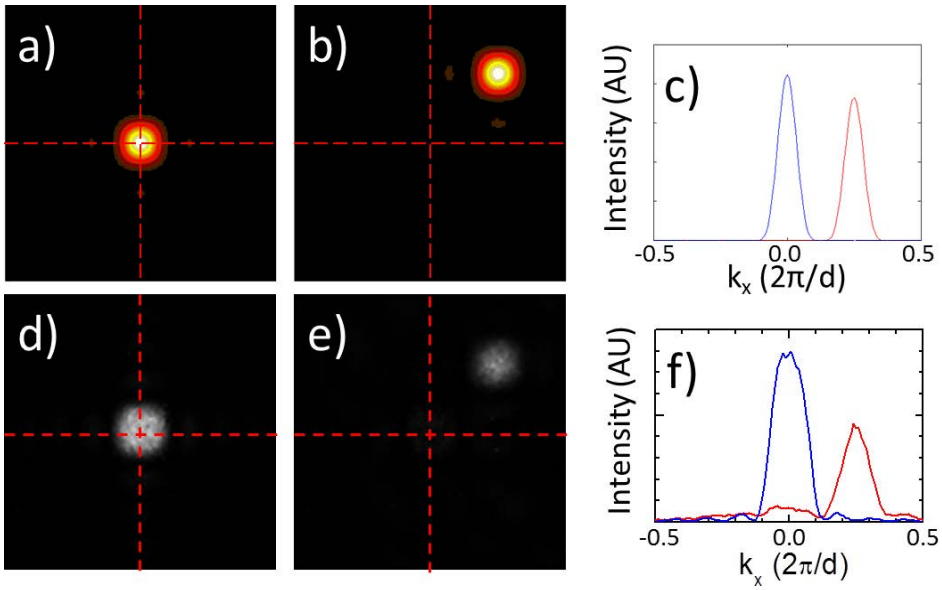

Fig. 8. Calculated and measured far field patterns of reflected light from the phased array. Calculated reflection from (a) a flat array, (b) a diagonal phase gradient and (c) their cross section plotted together. Measured reflection from (d) a flat array, (e) a diagonal phase gradient and (f) their cross section plotted together.

contribution of zeroth order light from the device substrate and subtracted it from the measurements to show contrast in the steered beam. The similarities between the far field pattern and the calculations verify the effectiveness of our closed loop feedback system.

Most of our optical power is lost since the mirrors only cover a small portion of the incident beam. As stated earlier, the HCG mirrors have 20 μm widths on a 35 μm mirror pitch. A 332 μm diameter Gaussian spot illuminates the array, overfilling it for an inherent 7.03 dB insertion loss. Since the fill factor is small, we choose to use the system without a Faraday rotator to eliminate the background light. We measure 7.12 dB insertion loss after correcting for the 50% power throughput caused by the absence of a Faraday rotator. We can decrease the insertion loss in two ways: by increasing the mirror fill factor and by decreasing the spot size relative to the array. Increasing the fill factor will also increase diffraction efficiency by decreasing the power in the side lobes. To decrease the relative spot size, the beam spot size can be reduced or the array size can be expanded with either larger mirrors or more array elements. Expansion of the mirrors leads to the expansion of the array period, and the spatial frequency of the array decreases along with the total beamsteering range. This also creates heavier MEMS HCG mirrors which slow down the operation speed. The preferable alternative is to add more mirrors to the array which also creates a less divergent beam; the tradeoff for this is additional complexity in the fabrication and control of more mirrors. This modification will be presented in future publications.

Figure 9 shows the superposition of 16 camera images taken while the beam is directed to 16 angles on a rectangular grid to demonstrate the beamsteering accuracy. Their positions are defined by the centroids of each beam. From these positions, we calculate 2.5% rms departure from the square lattice. While not obvious in the figure, pincushion aberrations from the lenses contribute to this error. These are correctable through software calibration of the beam deflection angle.

Similar to the stroboscopic measurements of individual mirror phase response, we took stroboscopic measurements of the far field by projecting it onto the camera sensor and synchronizing the drive voltage to the camera frame rate. A binary phase checkerboard pattern was used with a single voltage level to create 4 first order diffraction spots in the far

#180849 - $15.00 USD Received 30 Nov 2012; revised 17 Jan 2013; accepted 22 Jan 2013; published 29 Jan 2013

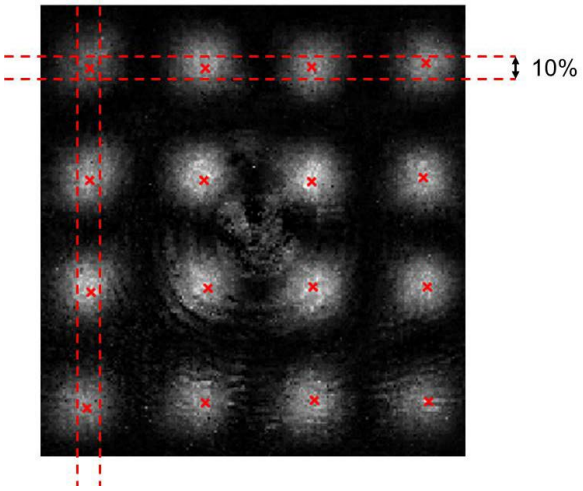

Fig. 9. 16 camera images of diffracted beams superimposed onto one image, with the 0th order beam subtracted. The red x's indicate the centroid of each beam to show the pointing error.

field. We integrated the intensity of the diffracted and central beams to plot their transient response, as shown in Fig. 10. As with single mirror displacement, this also exhibited damped harmonic oscillations. In this case, an overshoot in the mirror displacements leads to a loss of diffraction efficiency and decrease in measured diffracted power. This ceiling effect produces an oscillating intensity with twice the resonance frequency. With this accounted for, we measured 182 kHz resonances with a 2.2 μs damping coefficient with pull down. These measurements are 317 kHz resonances with 2.8 μs damping coefficient with release. This is three times faster than previously reported MEMS pistons mirror arrays [10]. Figure 10(c) also reveals higher diffraction orders that mainly result from the imperfect fill factor of the mirror array. These can be reduced by designing a higher fill factor.

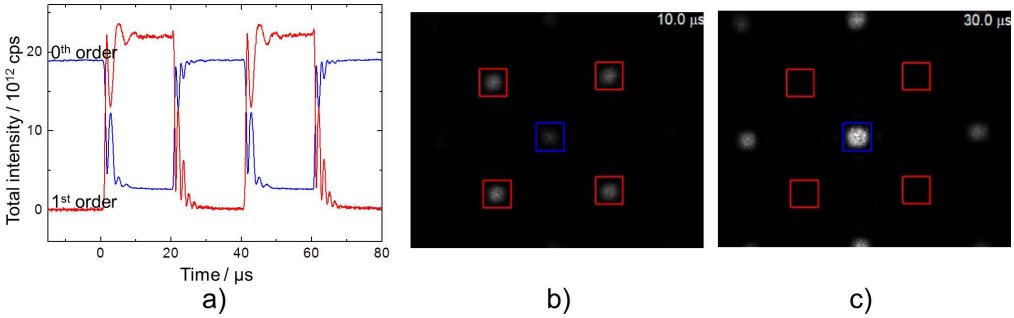

Fig. 10. (a) Transient response of the far field pattern when a checkerboard pattern is applied with a square wave. The blue and red boxes in the far field pattern indicate the integration areas from which we calculate the intensity levels. Shown here are the far field patterns at (b) 10 μs and (c) 30 μs.

4. Conclusion

We developed a beamsteering system which provides closed-loop feedback control of a two-dimensional optical phased array of high contrast grating mirrors. Closed loop feedback is accomplished simultaneously with device output, using only a small percentage of the optical power. Individual mirror calibration becomes unnecessary as closed loop feedback only requires the definition of phase setpoints. This feedback also allows for in situ correction of phase drift that occurs with device use and environmental changes. With this system, we

#180849 - $15.00 USD Received 30 Nov 2012; revised 17 Jan 2013; accepted 22 Jan 2013; published 29 Jan 2013

demonstrated $<\pi/100$ phase control accuracy and performed beamsteering with better than 2.5% pointing accuracy. Stroboscopic measurements by gated imaging reveal the dynamic response of the mirror motion and far field response, showing damped harmonic motion with 320 kHz resonance. The ability to measure the dynamic response allows us to show the elimination of the harmonic motion using feedforward waveform shaping.

Acknowledgments

The authors would like to acknowledge support from the DARPA SWEEPER program.

#180849 - $15.00 USD Received 30 Nov 2012; revised 17 Jan 2013; accepted 22 Jan 2013; published 29 Jan 2013